Available online at www.sciencedirect.com
ScienceDirect
Carbohydrate Research 342 (2007) 1470–1479
Carbohydrate RESEARCH

The glass transition temperatures of amorphous trehalose–water mixtures and the mobility of water: an experimental and in silico study

Alexandra Simperler,[a] Andreas Kornherr,[b,*] Reenu Chopra,[a] William Jones,[a,*] W. D. Samuel Motherwell[c] and Gerhard Zifferer[b]

[a]*The Pfizer Institute for Pharmaceutical Materials Science, Department of Chemistry, University of Cambridge, Lensfield Road, Cambridge CB2 1EW, UK*
[b]*Institute of Physical Chemistry, University of Vienna, Währinger Strasse 42, A-1090 Wien, Austria*
[c]*Cambridge Crystallographic Database Centre, 12 Union Road, Cambridge CB2 1EZ, UK*

Received 27 November 2006; received in revised form 6 April 2007; accepted 11 April 2007
Available online 27 April 2007

Abstract—Isothermal–isobaric molecular dynamics simulations are used to calculate the specific volume of models of trehalose and three amorphous trehalose–water mixtures (2.9%, 4.5% and 5.3% (w/w) water, respectively) as a function of temperature. Plots of specific volume versus temperature exhibit a characteristic change in slope when the amorphous systems change from the glassy to the rubbery state and the intersection of the two regression lines provides an estimate of the glass transition temperature T_g. A comparison of the calculated and experimental T_g values, as obtained from differential scanning calorimetry, shows that despite the predicted values being systematically higher (about 21–26 K), the trend and the incremental differences between the T_g values have been computed correctly: $T_g^{5.3\%\ (w/w)} < T_g^{4.5\%\ (w/w)} < T_g^{2.9\%\ (w/w)} < T_g^{0.0\%\ (w/w)}$. The mobility of water has been investigated over temperature ranges covering the rubbery and the glassy phases of the trehalose–water mixtures by calculating the diffusion coefficients of water. The temperature dependence of the diffusion coefficient changes in the region of the glass transition and can be used as well to estimate T_g values. The activation energies for water diffusion were found to be independent of the amount of water in amorphous trehalose.

Keywords: Amorphous trehalose–water mixtures; Differential scanning calorimetry; Diffusion; Glass transition temperatures; Molecular dynamics simulations

1. Introduction

Amorphous carbohydrates are often employed in the pharmaceutical and food industries to effectively encapsulate, stabilise and ultimately release labile pharmaceutically active materials. They possess advantageous properties such as being readily available with high purity, low toxicity, good glass-formers and have high glass transition temperatures (T_g).[1,2] At temperatures below T_g, in the so-called glassy state, molecular mobility is sharply reduced. High viscosity of the system slows the relaxation time down dramatically and the amorphous formulation gains physical stability.[1] The higher the T_g value of an amorphous formulation the higher the temperature to which the physical stability can be extended. Thus, encased in a high T_g amorphous carbohydrate, pharmaceutical products may be stored at room temperature and shipped without cooling. For example, the disaccharide trehalose (Scheme 1) is widely used for this purpose due to its relatively high glass transition temperature and low tendency to crystallise.[1–4]

* Corresponding authors. Tel.: +43 0 1 4277 52434 (A.K.); tel.: +44 0 1223 336468 (W.J.); e-mail addresses: andreas.kornherr@univie.ac.at; wj10@cam.ac.uk

0008-6215/$ - see front matter © 2007 Elsevier Ltd. All rights reserved.
doi:10.1016/j.carres.2007.04.011

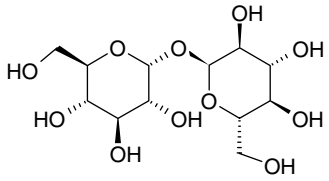

α,α-Trehalose –
α-D-Glucopyranosyl, α-D-Glucopyranoside

Scheme 1. Structure of trehalose.

In general, carbohydrates are hydrophilic and tend to strongly interact with water, which they may absorb either during the manufacturing process of a pharmaceutical formulation or from their surrounding after manufacture. Water can act as plasticizing agent changing the key mechanical properties and depressing the glass transition temperature of an amorphous carbohydrate.[2,5] Furthermore, water may also affect the degradation of the actual drug embedded in the carbohydrate excipient.[6] Thus, structural and dynamic properties such as distribution, diffusion, mobility, etc., of water in amorphous carbohydrates have been a subject of great interest to both experimentalists[7–17] and theoreticians.[18–28]

The main aim of this study was to investigate if modelling is capable of reproducing the reduction of T_g values with increasing water content which has been observed by differential scanning calorimetry (DSC) measurements in amorphous trehalose–water mixtures with a water content of 0–5.4% (w/w). In addition, the temperature dependency of the water diffusion coefficients D was investigated over selected temperature ranges, which covered the rubbery and glassy phases of the trehalose–water mixtures.

The glass transition temperatures were obtained by simulating the cooling of an amorphous solid by performing a series of isothermal–isobaric molecular dynamics (MD) simulations at set temperatures. Experiments have shown that the thermal expansivity of an amorphous system will decrease at its T_g when it passes from a rubbery to a glassy state.[8,29,30] Thus, a lower rate of decrease of the specific volume v_{spec} with decreasing temperature may be expected below T_g. Therefore, a plot of v_{spec} against temperature shows a change in slope and T_g can be identified at the intersection of two regression lines. This phenomenon is the foundation of the so-called free volume theory,[31,32] where the (free) volume and the density are the main controlling parameters determining the dramatic slowing down of the structural relaxation times at and below the glass transition temperature.[33] This method is often applied to model T_g values of polymers, carbohydrates and carbohydrate–water mixtures.[22–24,34–44]

Simulations will, however, overestimate the T_g values[18,45] since values are dependent on cooling rates.[46] In typical DSC experiments cooling rates are in the range of minutes whereas for molecular dynamics the cooling rate is in the nanosecond range. Thus, we do not expect the calculated T_g values to be identical to the T_g values obtained from DSC measurements. We do, however, expect that the incremental changes of the modelled set of T_g values will be comparable to the experimental values.

The diffusion coefficients of water were obtained from the mean square displacement (MSD) of the water oxygen atoms at a particular temperature using the Einstein relation[47] (see below). This approach is one of the most frequently used in determining diffusion coefficients by MD simulations.[20,22,23,35,39,48] The temperature dependency of the water diffusion coefficient changes in the glass transition range[14,16,25,27,39] and is another source of predicting T_g values. Accordingly, the quality of this approach is also analysed and the dependency of the activation energy of diffusion on the water content of amorphous trehalose is discussed.

2. Methods

2.1. Experimental methods

Trehalose was commercially available as α,α-D-(+)-trehalose dehydrate crystalline powder from Fluka (≥99.0% purity). To obtain the anhydrous amorphous trehalose sample, freeze-drying was performed using a VirTis AdVantage benchtop freeze-dryer. Additionally, trehalose samples were prepared containing 2.9%, 4.5% and 5.3% (w/w) water by placing the anhydrous trehalose samples in desiccators where different relative humidities (RH) were maintained with standardised saturated salt solutions (Table 1).

The trehalose samples (5–10 mg) were placed in DSC pans and were sealed inside a glove box, which was kept at a relative humidity below 0.5% using regenerated molecular sieves. For all DSC measurements, a Mettler Toledo STAR DSC822^e differential scanning calorimeter was used with nitrogen purge at 50 cm^3/min. An indium calibration was used ($T_m = 429.60 \pm 0.3$ K, heat of fusion $= 28.45 \pm 0.6$ J/g), and the samples (ca. 2–10 mg) were analysed in crimped aluminium pans (40 and 100 μL).

Table 1. Details of used trehalose–water mixtures

%RH	Saturated salt solution	% (w/w) H_2O	Corresponds to:
11	LiCl	2.9	$41H_2O$ + 72 trehalose molecules
22	$CH_3COO^-K^+$	4.5	$64H_2O$ + 72 trehalose molecules
33	$MgCl_2$	5.3	$77H_2O$ + 72 trehalose molecules

Using DSC, the heat capacity C_p of a sample can be monitored, which resembles the change of the enthalpy H of a system with respect to temperature:[49]

$$C_p = \partial H(T)/\partial T \quad (1)$$

The integral over the experimentally obtained DSC cooling traces,

$$\int C_p \, dT = H(T) + \text{const} \quad (2)$$

was used to determine the glass transition temperatures. The resulting H (short hand for $H(T) + \text{const}$) against temperature plots graphically resemble the v_{spec} versus T plots as obtained from calculations: curves with a shallow inflexion. The experimental values of T_g (referred to as T_g^{exp}) were then obtained by fitting regression lines through the low and high temperature branches of these curves and determining their intersections.

2.2. Computational methods

2.2.1. Calculation of T_g values. The molecular structure of trehalose was extracted from the Cambridge Structural Database (CSD).[50,51] No specific conformers of the trehalose molecules were considered and all structures were kept fully flexible during the whole MD process. The amorphous model systems of trehalose and the trehalose–water mixtures were built with the Amorphous Cell tool as implemented in the Materials Studio 3.0™ simulation package from Accelrys.[22] Seventy-two molecules of trehalose were used to generate a model for anhydrous trehalose whereas for the trehalose–water mixtures 41, 64 and 77 water molecules where added to obtain models with 2.9%, 4.5% and 5.3% (w/w) water, respectively. In total, three cubic cells (with periodic boundaries in all directions) of 3.0 nm × 3.0 nm × 3.0 nm (Fig. 1) were built for anhydrous trehalose and each of the mixtures. Thus, three independent data sets (referred to as data sets I, II and III) were available for the determination of a particular glass transition temperature.

These cells were relaxed for 2 ns under isobaric–isothermal conditions (NPT ensemble) at a temperature of about 100 K above the experimental T_g values (i.e., 470, 460, 470 and 450 K for trehalose with 0%, 2.9%, 4.5% and 5.3% (w/w) water, respectively) using periodic boundary conditions. The final configurations of these MD runs were used as starting structures for a cooling cycle where the temperature was decreased in 10 K steps until a temperature of at least 100 K below the experimental T_g value was reached (i.e. 270, 240, 200 and 170 K for trehalose with 0%, 2.9%, 4.5% and 5.3% (w/w) water, respectively). At each temperature, a NPT MD run was carried out for 200 ps, where 150 ps allows for equilibration and the last 50 ps is used for data sampling. The final configuration of each individual 200 ps run was extracted and subsequently used as starting structure for the following run. Every ps, the specific density, ρ_{spec}, was sampled from the last 50 ps of each run and the average value over these 50 data points was taken as the result. Plots of ρ_{spec} versus simulation time t (Fig. 2) for a model of 72 trehalose and 64 water molecules (for three different temperatures) show that all ρ_{spec} values are well equilibrated within the chosen simulation period of 200 ps. Finally, the specific volumes

$$v_{spec} = 1/\rho_{spec} \quad (3)$$

were calculated and plotted versus temperature.

All MD simulations were performed with DISCOVER[22] using the COMPASS[52–55] force field. The Anderson

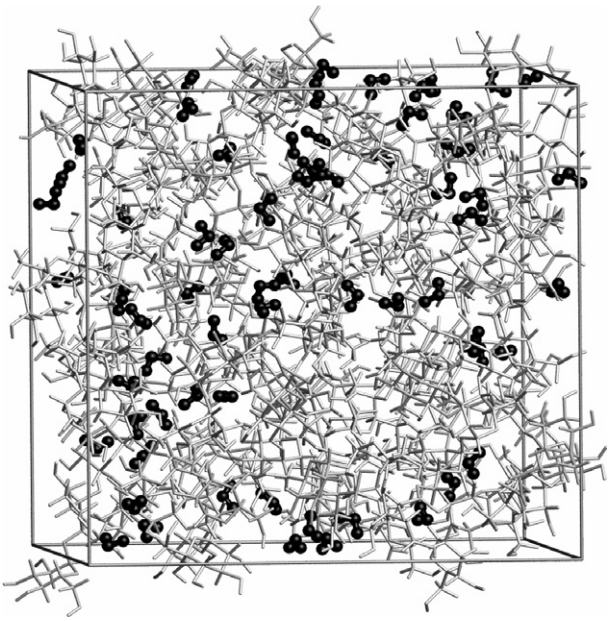

Figure 1. Cubic cell with 75 molecules of trehalose (grey) and 64 molecules of water (black).

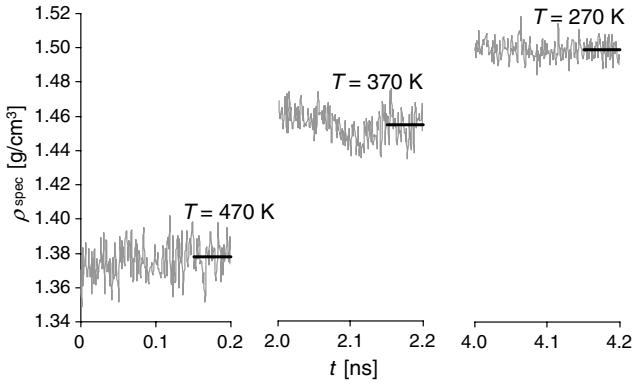

Figure 2. Plot of ρ_{spec} versus simulation time, t, for 75 molecules of trehalose and 64 molecules of water for three different temperatures: $T = 470$ K (start-temperature), $T = 370$ K (near T_g) and $T = 270$ K (near end). The average ρ_{spec} values over the last 50 ps (visualised by bold lines) are given within the figure.

thermostat and barostat[56] were employed with a time step of 1 fs. The cutoffs (with a cutoff radius of 1.25 nm) for the computation of energies and forces for the electrostatic as well as van der Waals interactions (employing a Lennard-Jones 9-6 function) were charge group based to avoid erroneous monopole–monopole terms.

2.2.2. Calculation of diffusion coefficients. The diffusion coefficients of water were modelled for trehalose with 2.9%, 4.5% and 5.3% (w/w) of water over a temperature range, which covered the rubbery and glassy phases of these systems. Therefore, the final configuration of each individual cooling run was taken and exposed to 50 ps MD under isochoric–isothermal conditions (NVT ensemble) at the respective temperatures. For each of the trehalose–water mixtures, the NVT-MD runs were performed on configurations of all three cooling runs to have three independent data sets (referred to as data sets I, II and III) available for the determination of a particular diffusion coefficient. During the MD-runs, data were sampled every 0.5 ps. The diffusion coefficient D of water at a particular temperature can be evaluated from the limiting slope from a plot of mean square displacement (MSD) of the oxygen atom of water against time,

$$D = \frac{1}{6}\lim_{t\to\infty}\frac{\mathrm{d}[\mathrm{MSD}]}{\mathrm{d}t} \quad (4)$$

where

$$\mathrm{MSD} = \langle|\vec{r}_i(t) - \vec{r}_i(0)|^2\rangle \quad (5)$$

and $\vec{r}_i(t)$ is the position of the ith oxygen atom in the simulation box at a particular time t with angle brackets indicating mean values averaged over this period of time. The initial period of the NVT-MD runs is influenced by the input NPT-MD data, while the final time points is noted to show rather poor statistics, giving rise to large fluctuations.[22] Thus, the diffusion coefficient was obtained from a slope of a linear regression of data points in the range from 10 to 40 ps.

For reasons of comparison, the diffusion coefficient of water was calculated as well. An amorphous model ($999H_2O$ molecules in a cubic cell with the dimensions 3.13 nm × 3.13 nm × 3.13 nm, referring to a density of 1 g cm^{-1}) was built with the Amorphous Cell tool.[22] The model had to undergo similar treatment to the trehalose–water models and due to the fact that water molecules are small the simulation times could be reduced in some cases. The cubic cell was relaxed under periodic boundary conditions for 1 ns under NPT conditions at a temperature of 170 K. The final configurations of these MD runs were used as starting structures for a heating cycle where the temperature was increased in 10 K steps until a temperature of 390 K, which is below the boiling point of water. Calculating a cooling cycle was not possible as a relaxation at 390 K resulted in a massive expansion of the cell. At each temperature, a NPT MD run was carried out for 100 ps, and the final conformations of each run were used to perform the 50 ps NVT-MD runs to obtain the diffusion coefficient of water. We obtained a diffusion coefficient of 4.4×10^{-9} m^2 s^{-1} (at 300 K and 1 atm), which overestimated the experimental value of 2.14×10^{-9} m^2 s^{-1} (at 298 K and 1 atm).[57] The modelling of diffusion coefficients is still difficult because it is highly sensitive to the modelling conditions,[58] such as choice of ensemble, thermostat, cutoff radii, force field, etc.

In order to avoid artificially rescaling of velocities (which plays no role for structure and energy but is crucial for dynamics of a given system) the Nosé[59] instead of the Anderson[56] thermostat was used.

3. Results

3.1. Comparison of experimental and calculated T_g values

For each of the four amorphous trehalose samples, examples of experimental DSC cooling traces and corresponding integrals (Fig. 3a–d, upper and lower plots) are shown. The regression lines employed to determine the glass transition temperature are shown in the H against temperature plots and the T_g values are indicated: 368, 329, 312 and 304 K for trehalose with 0.0%, 2.9%, 4.5% and 5.3% (w/w) water, respectively. The decrease of T_g with an increasing amount of water has been proven to be reproducible with experimental methods.

The procedure of obtaining T_g values from MD simulations by plotting the average specific volume of three independent amorphous models against temperature was discussed by the authors in more detail elsewhere.[18] Following this procedure, three data sets I, II and III (Fig. 4, open symbols, upper plots) were used to obtain average v_{spec} values (Fig. 4, closed symbols, upper plots) for each of the amorphous trehalose and three trehalose–water mixtures. Such plots contain a kink in the glass transition region as above T_g (rubbery phase) the specific volume will increase more rapidly with increasing temperature than below T_g (glassy phase). Therefore, the calculated data have to be split into a glass-set and a rubbery-set so that two linear regression lines can be obtained. The intersection of these two lines allows the determination of T_g; due to the higher kinetic energy, which naturally occurs at higher temperatures, the scattering of data points is more pronounced in the rubbery phase than in the glassy phase. Thus, the allocation of data points near T_g is made especially difficult. However, it was found[18,34] that taking the average (Fig. 4, closed symbols, upper plots) over the three data sets gave a great improvement considering the level of

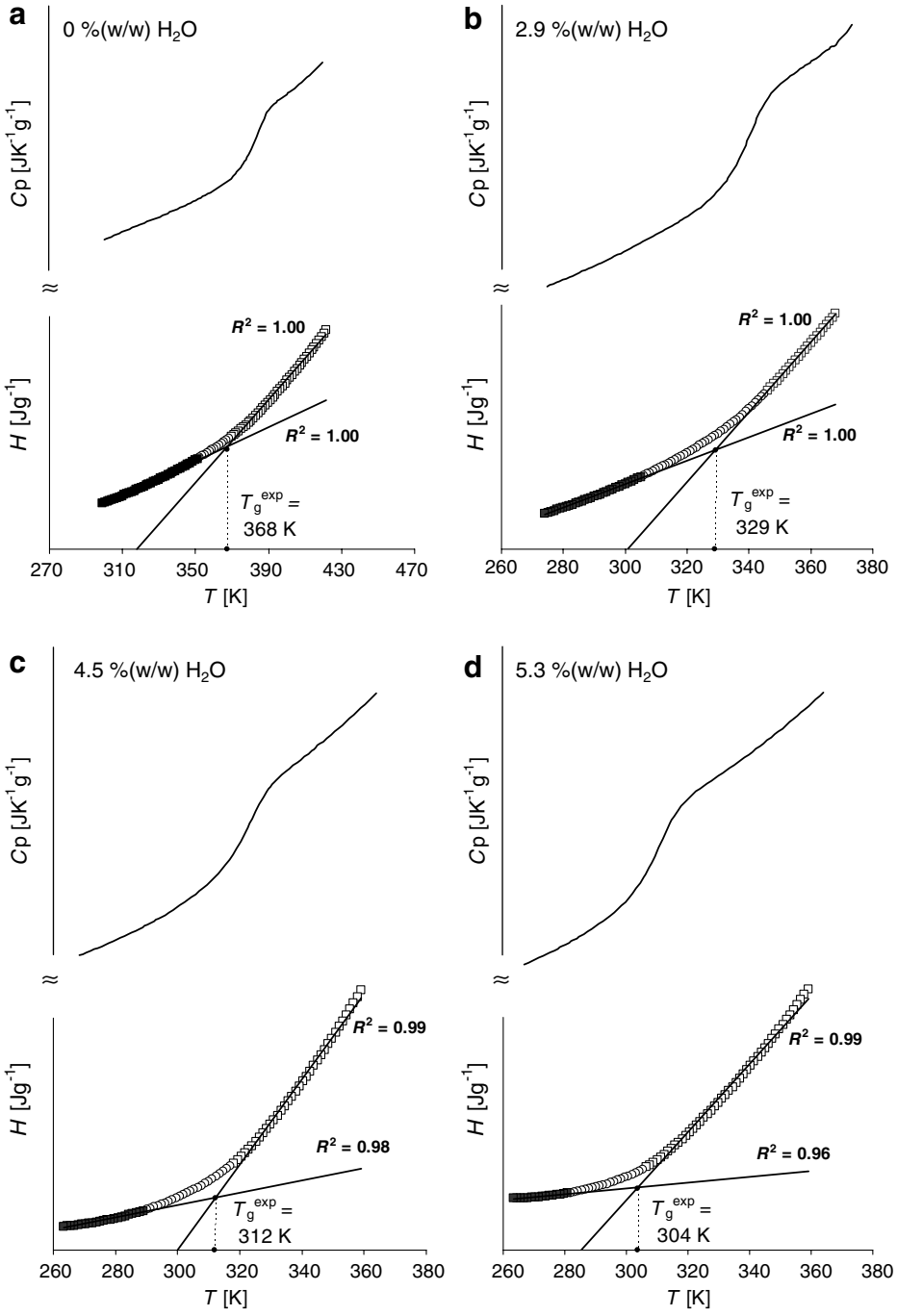

Figure 3. Experimental DSC traces of trehalose with (a) 0.0%, (b) 2.9%, (c) 4.5% and (d) 5.3% (w/w) of water. Upper plot: DSC cooling trace $\partial H(T)/\partial T$ versus temperature T. Lower plot: integral of the DSC trace H versus temperature T. Fit of two linear regression lines through the data points of the glass branch (■) and the data points of the rubber branch (□). T_g values are indicated at their intersection. All data points which were not used for fitting the regression lines are indicated with ○.

scattering. The allocation of data points to either the glass- or rubber-set was also less ambiguous using the averaged data. Accordingly, all data points were successfully separated into a glass- (Fig. 4, closed squares, lower plot) and a rubber-set (Fig. 4, open square, lower plot). The intersection of the two resulting linear regression lines indicates the change of slope within the v_{spec} against T plot; this gives T_g values of 392, 350, 338 and 327 K for trehalose with 0.0%, 2.9%, 4.5% and 5.3% (w/w) water, respectively.

Table 2 compares the experimental T_g^{exp} to the calculated T_g^{calc} values and in Figure 5 the experimental are plotted against the calculated values. The experimental sequence of the T_g values has been correctly

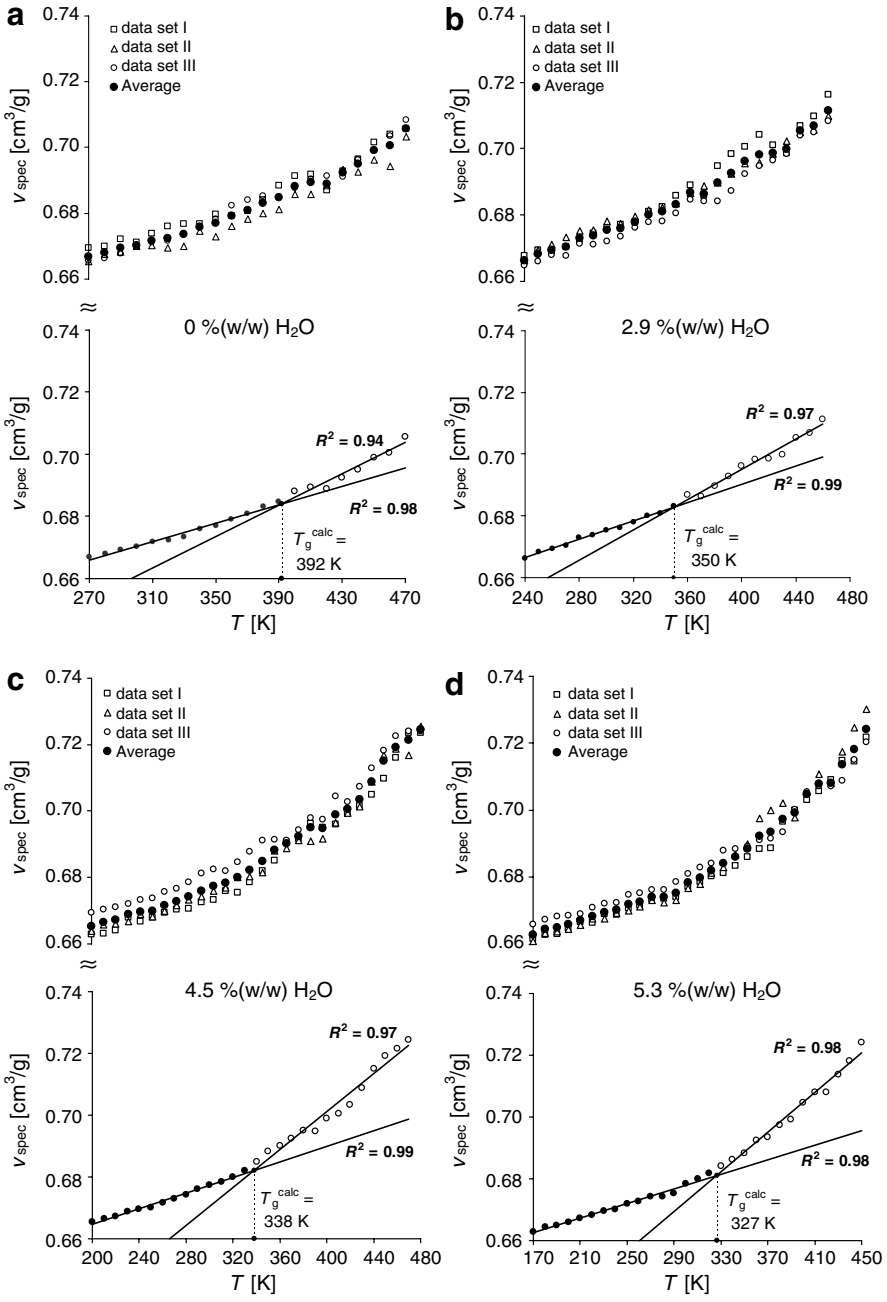

Figure 4. Calculated v_{spec} versus T plots of trehalose with (a) 0.0%, (b) 2.9%, (c) 4.5% and (d) 5.3% (w/w) of water. Upper plot: v_{spec} data of three independent data sets (open symbols) along with average v_{spec} data (closed symbols). Lower plot: fit of two linear regression lines through the v_{spec} data points of the glass branch and the data points of the rubber branch; T_g is indicated at their intersection. The correlation coefficient R^2 of the linear regressions is directly given in the plots.

predicted by our simulations: $T_g^{5.3\%\ (w/w)} < T_g^{4.5\%\ (w/w)} < T_g^{2.9\%\ (w/w)} < T_g^{0.0\%\ (w/w)}$. The calculated T_g values of trehalose with 0.0%, 2.9%, 4.5% and 5.3% (w/w) water are 24, 21, 26 and 23 K above their corresponding T_g^{exp} values. As stated previously in the introduction, the extremely fast cooling rates of MD simulations are responsible for this overestimation of calculated T_g values with respect to the experimental values. Nevertheless, the MD calculations noticeably resemble the sequence and incremental changes between the individual T_g values. An exact agreement is not to be expected since the experimental and simulation systems are in effect quite different and neither in a state of equilibrium. The different cooling rates cause the glass transitions for the experimental and simulated systems to differ by 21–26 K. However, what we can expect is that the incremental changes are correctly computed and this is clearly the case.

Table 2. Measured and calculated glass transition temperatures

% (w/w) H_2O	T_g^{exp} (K)	T_g^{calc} (K)
0.0	368	392
2.9	329	350
4.5	312	338
5.3	304	327

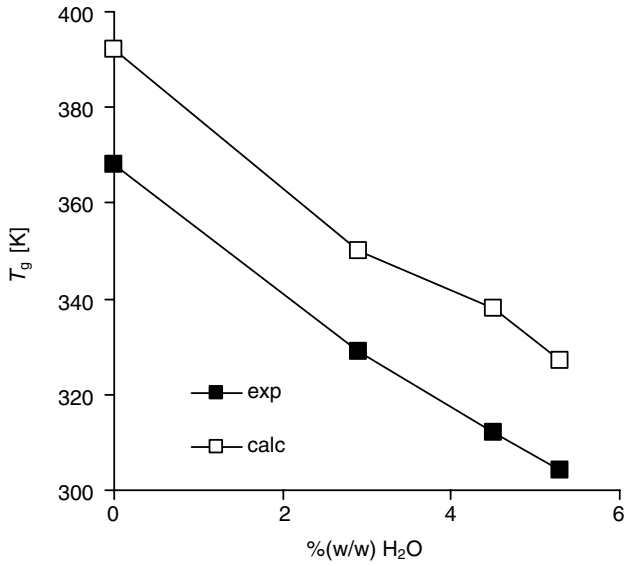

Figure 5. Experimental and calculated T_g values plotted versus % (w/w) water: T_g^{exp} (closed symbols) and T_g^{calc} (open symbols).

3.2. Diffusion coefficients of water

For each of the three amorphous trehalose–water mixtures, the diffusion coefficient of water, D, was obtained (Section 2.2.2.) as a function of temperature. In Figure 6a–c, D of all three amorphous models (data sets I, II and III, open symbols) and the average of the three data sets (closed symbols) are plotted against temperature. T_g values, which were previously obtained from the temperature dependency of v_{spec}, are indicated with black lines (Fig. 6a–c). For all trehalose–water mixtures reported here, the water diffusion coefficients decrease almost linearly with decreasing temperature in the rubbery phase until the respective glass transition temperature is reached. Below T_g, the values are almost zero. However, there is some evidence that small molecules such as water are not totally immobile below T_g; they may still undergo diffusion via 'hopping' between interconnected voids left in a carbohydrate polymer matrix after the glass transition.[13,16,21,60,61] Given that the water contents used in this study are very low it may be that diffusion below T_g is underestimated.

This temperature dependence of D for water in amorphous carbohydrates has been discussed in several scientific studies[14,16,25,27,39] and has also been used as a further method to determine the T_g values of a system. For the sake of comparison, this method was applied to the trehalose–water mixtures under consideration and Figure 6d–f show the average D values separated into a glass (closed squares) and a rubber-set (open square). The intersection of the two resulting linear regression lines indicates the change of slope within the D against T plot; this gives T_g^{diff} values in the correct sequence of 366, 351 and 344 K for trehalose with 2.9%, 4.5% and 5.3% (w/w) water, respectively. The calculated T_g^{diff} values are 16, 13 and 17 K above the calculated T_g^{calc} values and 37, 39 and 40 K above the experimental T_g^{exp} values. The scattering of D values of the rubber-set is much stronger than the scattering of the v_{spec} values. Therefore, the inflexion points of v_{spec} against T plots are more reliable in the prediction of T_g.

Furthermore, in Figure 7 the diffusion coefficients are plotted in a semi-logarithmic plot against $1/T$: the plot leads to the assumption that the temperature dependency of D roughly follows an Arrhenius-type law

$$D(T) = D_0 e^{(-\Delta E_{act}/RT)} \quad (6)$$

The emergence of a linear Arrhenius dependency has been previously reported in experimental studies.[13,14,16] Linear regression lines for $\ln D$ against $1/T$ have been fitted with R^2 values of 0.90, 0.94 and 0.92 Å for trehalose–water mixtures with 2.9%, 4.5% and 5.3% (w/w) water. The activation energies using Eq. 6 resulted in $E_{act}^{2.9\%\ (w/w)} = 17$ kJ/mol, $E_{act}^{4.5\%\ (w/w)} = 20$ kJ/mol and $E_{act}^{5.3\%\ (w/w)} = 17$ kJ/mol showing no significant difference. Thus, they are independent of the water content, which is in agreement with the findings of Tromp et al.[13]

4. Conclusions

The temperature dependency of the specific volumes of amorphous trehalose and trehalose–water mixtures (i.e. 0.0%, 2.9%, 4.5% and 5.3% (w/w) water) was successfully modelled with NPT molecular dynamics simulations by simulating a cooling process. To reduce the scattering of calculated v_{spec} data especially in the higher temperature range, three independent models were used to generate one set of average v_{spec} for each of the mixtures. The calculated T_g values were obtained by locating the inflexion points of the v_{spec} against T plots by fitting linear regression lines. A comparison of the calculated data with experimental data as obtained from DSC cooling traces revealed that the trend of the T_g values was calculated correctly: $T_g^{5.3\%\ (w/w)} < T_g^{4.5\%\ (w/w)} < T_g^{2.9\%\ (w/w)} < T_g^{0.0\%\ (w/w)}$. Due to much faster cooling rates in the simulations, the calculated T_g values are 21–26 K above the experimental values. However, the trend and the incremental changes between the experimental T_g values were precisely predicted by our simulation, which was the main aim of this study. Thus, modelling could be effectively used to predict T_g values of carbo-

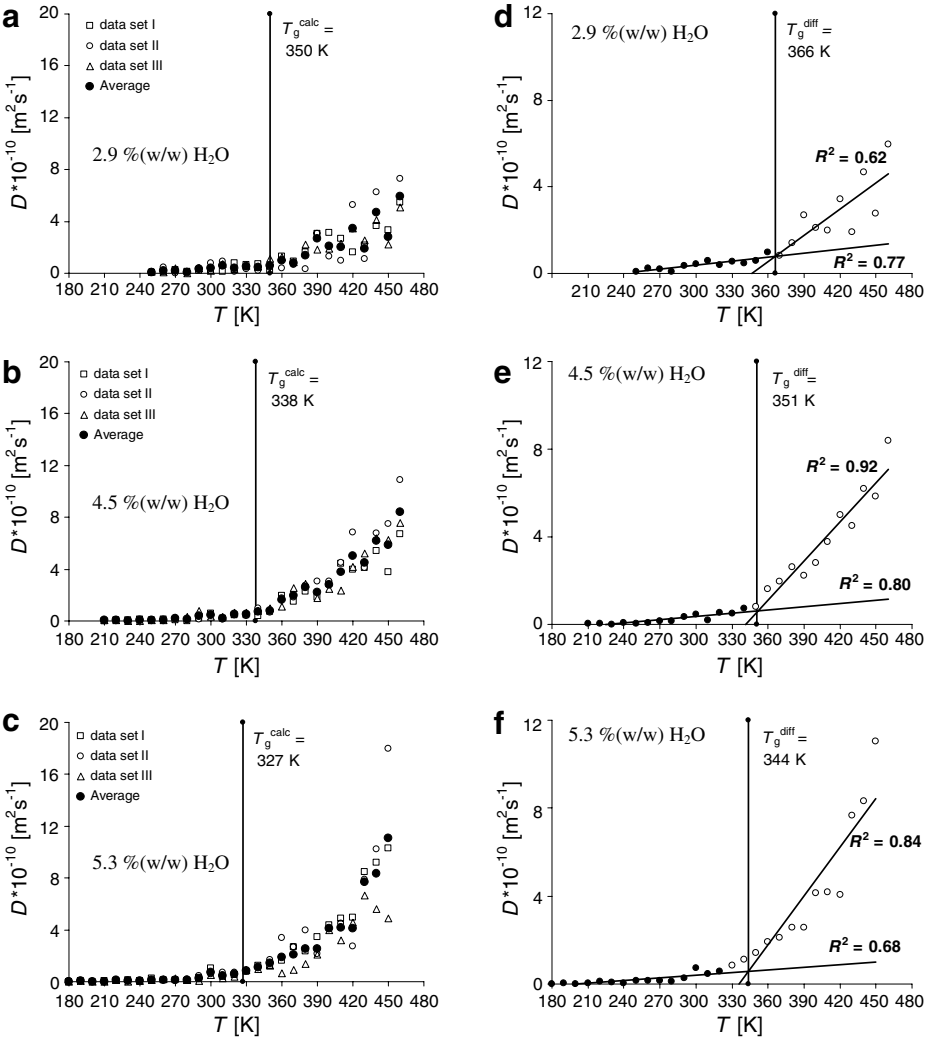

Figure 6. Calculated D versus T plots of trehalose with (a, d) 2.9%, (b, e) 4.5% and (c, f) 5.3% (w/w) of water: (a–c): D data of three independent models (open symbols) along with average D data (closed symbols). The indicated T_g values were obtained from the v_{spec} versus T plots. (d–f): fit of two linear regression lines through the D data points of the glass branch and the data points of the rubber branch; T_g^{diff} is indicated at their intersection. The correlation coefficient R^2 of the linear regressions in this and the following figures is directly given in the plots.

hydrate–water mixtures, which are unsuitable for DSC measurements due to decomposition.

The temperature dependency of the water diffusion coefficient of the trehalose–water mixtures was obtained by calculating the mean square displacement water subsequent to NVT molecular dynamics simulations over a range of temperatures, which covered both the rubbery and the glassy states. Similar to the above method, the kink in a plot of D against T was located by fitting two regression lines. The obtained T_g^{diff} values reproduce the experimental trend and incremental changes but overestimate the experimental values to a larger extent by 37–40 K. However, even the average D values obtained from three different models have a significant scattering in the rubbery range, which makes the fitting of a regression line difficult. Since this scattering may be improved only by very time-consuming computational

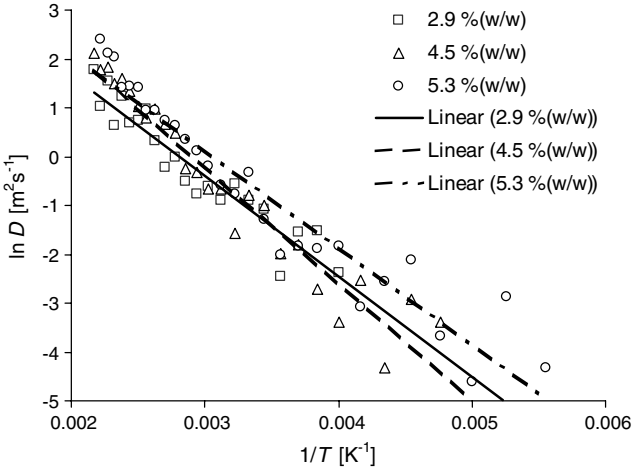

Figure 7. Semi-logarithmic plot of D versus $1/T$ for trehalose with 2.9% (□), 4.5% (△) and 5.3% (w/w) (○) of water. The three linear regression lines are indicated full, dashed and dashed-dotted for trehalose with 2.9%, 4.5% and 5.3% (w/w) of water.

relaxation periods, preference should be given to the v_{spec} against T method for estimating T_g values.

The diffusion coefficients of water molecules show an Arrhenius-like behaviour for all trehalose–water mixtures under consideration. The calculated activation energies of diffusion were quite similar and did not show any dependency on the amount of water in amorphous trehalose. This finding is in agreement with the fact that the activation energies are governed by the interconnected voids which are left when the trehalose molecules randomly pack in the amorphous glass.

Acknowledgement

The authors are grateful to the Pfizer Institute for Pharmaceutical Materials Science for financial support.

References

1. Hatley, R. H. M.; Blair, J. A. *J. Mol. Catal. B: Enzym.* **1999**, *7*, 11–19.
2. Hancock, B. C.; Shamblin, S. L. *PSTT* **1998**, *8*, 345–351.
3. Crowe, J. H.; Carpenter, J. F.; Crowe, L. M. *Annu. Rev. Physiol.* **1998**, *60*, 73–103.
4. Surana, R.; Pyne, A.; Suryanarayanan, R. *Pharm. Res.* **2004**, *21*, 867–874.
5. Hancock, B. C.; Zografi, G. *Pharm. Res.* **1994**, *11*, 471–477.
6. Shalaev, E. Y.; Zografi, G. *J. Pharm. Sci.* **1996**, *1996*, 1137–1141.
7. Kilburn, D.; Townrow, S.; Meunier, V.; Richardson, R.; Alam, A.; Ubbink, J. *Nat. Mater.* **2006**, *5*, 632–635.
8. Kilburn, D.; Claude, J.; Mezzenga, R.; Dlubek, G.; Alam, A.; Ubbink, J. *J. Chem. Phys. B* **2004**, *108*, 12436–12441.
9. Ahlquist, M. U. A.; Taylor, L. S. *J. Pharm. Sci.* **2002**, *91*, 690–698.
10. van den Dries, I. J.; van Dusschoten, D.; Hemminga, M. A.; van der Linden, E. *J. Phys. Chem. B* **2000**, *104*, 10126–10132.
11. Kajiwara, K.; Franks, F.; Echlin, P.; Greer, A. L. *Pharm. Res.* **1999**, *16*, 1441–1448.
12. Kajiwara, K.; Franks, F. *J. Chem. Soc., Faraday Trans.* **1997**, *93*, 1779–1783.
13. Tromp, R. H.; Parker, R.; Ring, S. G. *Carbohydr. Res.* **1997**, *303*, 199–205.
14. Champion, D.; Hervet, H.; Blond, G.; Le Meste, M.; Simatos, D. *J. Phys. Chem. B* **1997**, *101*, 10674–10679.
15. Noel, T. R.; Parker, R.; Ring, S. G. *Carbohydr. Res.* **1996**, *282*, 193–206.
16. Parker, R.; Ring, S. G. *Carbohydr. Res.* **1995**, *273*, 147–155.
17. Green, J. L.; Angell, C. A. *J. Phys. Chem.* **1989**, *93*, 2880–2882.
18. Simperler, A.; Kornherr, A.; Chopra, R.; Bonnet, P. A.; Jones, W.; Motherwell, W. D. S.; Zifferer, G. *J. Phys. Chem. B* **2006**, *110*, 19678–19684.
19. Choi, Y.; Cho, K. W.; Jeong, K.; Jung, S. *Carbohydr. Res.* **2006**, *341*, 1020–1028.
20. Lee, S. L.; Debenedetti, P. G.; Errington, J. R. *J. Chem. Phys.* **2005**, *122*, art. 204511.
21. Molinero, V.; Çagin, T.; Goddard, W. A., III. *Chem. Phys. Lett.* **2003**, *377*, 469–474.
22. Momany, F. A.; Willett, J. L. *Biopolymers* **2002**, *63*, 99–110.
23. Ekdawi-Sever, N. C.; Conrad, P. B.; de Pablo, J. J. *J. Phys. Chem. A* **2001**, *105*, 734–742.
24. Conrad, P. B.; de Pablo, J. J. *J. Phys. Chem.* **1999**, *A*, 4049–4055.
25. Caffarena, E. R.; Grigera, J. R. *Carbohydr. Res.* **1999**, *315*, 63–69.
26. Roberts, C. J.; Debenedetti, P. G. *J. Phys. Chem. B* **1999**, *103*, 7308–7318.
27. Caffarena, E. R.; Grigera, J. R. *Carbohydr. Res.* **1997**, *300*, 51–57.
28. Engelsen, S. B.; Pérez, S. *J. Mol. Graphics Modell.* **1997**, *15*, 122–131.
29. Kilburn, D.; Claude, J.; Schweizer, T.; Alam, A.; Ubbink, J. *Biomacromolecules* **2005**, *6*, 864–879.
30. Wang, H.; Ansems, P.; Chum, S. P.; Hiltner, A.; Baer, E. *Polym. Mater. Sci. Eng.* **2004**, *91*, 457–458.
31. Cohen, M. H.; Grest, G. S. *Phys. Rev. B* **1979**, *20*, 1077–1098.
32. Williams, M. L.; Landel, R. F.; Ferry, J. D. *J. Am. Chem. Soc.* **1955**, *77*, 3701–3707.
33. Floudas, G.; Mpoukouvalas, K.; Papadopoulos, P. *J. Chem. Phys.* **2006**, *124*, art. 074905.
34. Wagner, K. G.; Maus, M.; Kornherr, A.; Zifferer, G. *Chem. Phys. Lett.* **2005**, *406*, 90–94.
35. Xiang, T.-X.; Anderson, B. D. *Pharm. Res.* **2005**, *22*, 1205–1214.
36. Chen, W.; Lickfield, G. C.; Yang, C. Q. *Polymer* **2004**, *45*, 1063–1071.
37. Watt, S. W.; Chisholm, J. A.; Jones, W.; Motherwell, S. *J. Chem. Phys.* **2004**, *121*, 9565–9573.
38. Mazeau, K.; Heux, L. *J. Phys. Chem. B* **2003**, *107*, 2394–2403.
39. Yoshioka, S.; Aso, Y.; Kojima, S. *Pharm. Res.* **2003**, *20*, 873–878.
40. Yu, K.-Q.; Li, Z.-S.; Sun, J. *Macromol. Theory Simul.* **2001**, *10*, 624–633.
41. Yang, L.; Srolovitz, D. J.; Yee, A. F. *J. Chem. Phys.* **1999**, *110*, 7058–7069.
42. Fried, J. R.; Ren, P. *Comp. Theor. Polym. Sci.* **1999**, *9*, 111–116.
43. Caffarena, E. R.; Grigera, J. R. *J. Chem. Soc., Faraday Trans.* **1996**, *92*, 2285–2289.
44. Han, J.; Gee, R. H.; Boyd, R. H. *Macromolecules* **1994**, *27*, 7781–7784.
45. Buchholz, J.; Paul, W.; Varnik, F.; Binder, K. *J. Chem. Phys.* **2002**, *117*, 7364–7372.
46. Černošek, Z.; Holubová', J.; Černošková, E. *Solid State Sci.* **2003**, *5*, 1087–1093.
47. Einstein, A. *Ann. Phys.* **1905**, *17*, 549–560.
48. Fukuda, M. *J. Chem. Phys.* **1998**, *109*, 6476–6485.
49. Moynihan, C. T. *Rev. Mineral.* **1995**, *32*, 1–19.
50. Bruno, I. J.; Cole, J. C.; Edgington, P. R.; Kessler, M.; Macrae, C. F.; McCabe, P.; Pearson, J.; Taylor, R. *Acta Crystallogr., Sect. B* **2002**, *58*, 389–397.
51. Allen, F. H. *Acta Crystallogr., Sect. B* **2002**, *58*, 380–388.
52. Bunte, S. W.; Sun, H. *J. Phys. Chem. B* **2000**, *104*, 2477–2489.
53. Sun, H. *J. Phys. Chem. B* **1998**, *102*, 7338–7364.

54. Sun, H. *Macromolecules* **1995**, *28*, 701–712.
55. Hwang, M. J.; Stockfisch, T. P.; Hagler, A. T. *J. Am. Chem. Soc.* **1994**, *116*, 2515–2525.
56. Andersen, H. C. *J. Chem. Phys.* **1980**, *72*, 2384–2393.
57. Johnson, P. A.; Babb, A. L. *Chem. Rev.* **1956**, *56*, 387–453.
58. Pereira, J. C. G.; Catlow, C. R. A.; Price, G. D. *J. Phys. Chem. A* **2001**, *105*, 1909–1925.
59. Nosé, S. *Mol. Phys.* **1984**, *52*, 255–268.
60. Hills, B. P.; Wang, Y. L.; Tang, H. R. *Mol. Phys.* **2001**, *99*, 1679–1687.
61. Gunning, Y. M.; Parker, R.; Ring, S. G. *Carbohydr. Res.* **2000**, *329*, 377–385.